PROCEEDINGS, Thirty-Third Workshop on Geothermal Reservoir Engineering
Stanford University, Stanford, California, January 28-30, 2008
SGP-TR-185

A THREE-DIMENSIONAL POROELASTIC MODEL FOR WATER INJECTION INTO A GEOTHERMAL RESERVOIR

X. Zhou and A. Ghassemi

Texas A&M University
3116 TAMU-401E Richardson Building
College Station, TX, USA
e-mail: ahmad.ghassemi@pe.tamu.edu

ABSTRACT

A three-dimensional poroelastic model is developed to investigate the poroelastic effect of fluid injection into a geothermal reservoir. In the model, the fluid flow in the fracture is assumed to be lubrication flow and modeled by the finite element method. The three-dimensional pore fluid diffusion in the reservoir and the induced stresses are modeled by the boundary integral equation method. The numerical results have been verified through comparing to the analytical solutions given in Nygren and Ghassemi (2006) for an infinite radial fracture problem. Thereafter, the numerical model is used to study the pore pressure and stress fields in the rock matrix resulting from injection/extraction in a circular fracture.

INTRODUCTION

The production of geothermal energy from low permeability reservoirs is achieved by water circulation in natural and/or man-made fractures, and is often referred to as enhanced or engineered geothermal systems (EGS). Cold water injection perturbs the in-situ stress state within the reservoir leading to fracture initiation and/or activation of discontinuities such as faults and joints which is often manifested as multiple microseismic events. Detection and interpretation of microseismic events using downhole receiver arrays (e.g., Brady et al., 1994; Warpinski et al., 1996) can be monitored and analyzed to provide useful information on the stimulated zone, fracture growth, and geometry of the geological structures and the in-situ stress state (Warpinski et al., 2001; Guiterez, 2003; Pine, 1984). Micro-seismic events are believed to be associated with rock failure in shear, and shear slip on new or pre-existing fracture planes (Peasron, 1981). Effective interpretation of micro-seismicity can benefit from the knowledge of the hydro-thermo-mechanical mechanisms associated with injection in the reservoir, and the resulting stress variations that play a key role in rock failure around the main hydraulic fracture. These include the stresses due to the opening of a hydraulic fracture, and thermoelastic and poroelastic stresses due to rock cooling and fluid leak-off into the rock mass.

In general, an injection-induced fracture problem consists of (1) fluid flow and heat transport within the fracture, (2) fluid flow in the matrix, (3) conductive and advetcive heat transport in the matrix, and (4) fracture propagation. Some solutions for problems involving the first three parts have been presented (Ghassemi and Zhang, 2006; Nygren & Ghassemi, 2006; Nygren at al., 2005). Most of these as well as other studies of the subject were based on some simplifications such as uniform pressure in line fractures, special reservoir geometry and one-dimensional fluid diffusivity in the reservoir, etc. Other 3D models use the finite element method (e.g., Kohl et al. 1995). A three-dimensional boundary element model has been developed by Ghassemi et al. (2007) to study the impact of thermal stresses on the reservoir matrix and the fracture without considering poroelastic effects.

In this paper, a three-dimensional poroelastic model is developed to study the poroelastic response of the reservoir to fluid injection into an irregularly-shaped fracture or a fractured zone (see Fig. 1). The fluid flow in the fracture is assumed to be lubrication flow and is modeled using the finite element method. The three-dimensional pore fluid diffusion in the reservoir and the induced stresses is treated by the boundary integral equation method; and the displacement discontinuity boundary element method is used to model the fracture itself. The adoption of the boundary element method eliminates the need for discretizing the reservoir to account for the three-dimensional effect of fluid diffusivity in the reservoir. Both the finite element method and the boundary element methods use the same mesh, and they are coupled.

GOVERNING EQUATIONS

The governing equations of the problem are briefly described below.

Fluid flow in fracture

The fracture is assumed to be flat (or with moderate curvature), of finite size but can be irregular in shape. The reservoir is assumed to be poroelastic and of infinite extent. In this paper, we assume that the flow in the fracture is laminar and governed by the lubrication flow equation:

$$\nabla_2 p(x,y,0,t) = -\frac{12\mu}{w^3(x,y)}\mathbf{q}(x,y,t) \qquad (1)$$

where ∇_2 is the gradient operator in the fracture plane, $p(x,y,0,t)$ the fluid pressure in the fracture, μ the fluid viscosity, $w(x,y)$ the fracture width, $\mathbf{q}(x,y,t)$ the fluid discharge, and A is the fracture plane. Assuming the fluid to be incompressible and the fracture aperture does not vary with time, the fluid continuity equation could be written as:

$$\begin{aligned}\nabla_2 \cdot \mathbf{q}(x,y,t) = -2v_l(x,y,t) + \\ Q_i(t)\delta(x-x_i,y-y_i) - Q_e(t)\delta(x-x_e,y-y_e)\end{aligned} \qquad (2)$$

where $\nabla_2 \cdot$ is the two-dimensional divergence operator, v_l the leak-off fluid from one side of the fracture wall into reservoir, $Q_i(t)$ and $Q_e(t)$ respectively the fluid injection and extraction rates, (x_i, y_i) and (x_e, y_e) injection and extraction well locations, and δ the Dirac delta function. Using Eqs. (1) and (2) to eliminate $\mathbf{q}$, yields

$$\begin{aligned}\nabla_2 \cdot \left[w^3(x,y)\nabla_2 p(x,y,0,t)\right] = 24\mu v_l(x,y,t) + \\ 12\mu\begin{bmatrix}-Q_i(t)\delta(x-x_i,y-y_i)+ \\ Q_e(t)\delta(x-x_e,y-y_e)\end{bmatrix}\end{aligned} \qquad (3)$$

Eq. (3) cannot be used solely to solve $p(x,y,t)$ in the fracture as the fluid leak-off rate v_l is unknown and related to the pressure in the fracture in the following way:

$$v_l(x,y,t) = -k\frac{\partial p(x,y,z,t)}{\partial n} \qquad (4)$$

where k is the rock permeability, γ_w the unit weight of the fluid and n the outward normal of the fracture. As the leak-off rate from the fracture to the reservoir $2v_l$ is just the fluid source intensity which is denoted by q_f in this paper, Eq. (3) can be rewritten as;

$$\begin{aligned}\nabla_2 \cdot \left[w^3(x,y)\nabla_2 p(x,y,t)\right] = 12\mu q_f(x,y,t) + \\ 12\mu\begin{bmatrix}-Q_i(t)\delta(x-x_i,y-y_i)+ \\ Q_e(t)\delta(x-x_e,y-y_e)\end{bmatrix}\end{aligned} \qquad (5)$$

Reservoir responses to fluid leak-off

The fluid leak-off from the fracture to the reservoir could induce pore pressure variations stresses in the reservoir. The reaction of the reservoir is governed by the poroelastic mechanisms. The pressure at the location (x,y,z) and time t due to an instantaneous unit point source at location (x',y',z') and time t' is given by (Cheng and Detournay, 1998):

$$p^{si}(x-x',y-y',z,t-t') = \frac{c}{\pi^{3/2}\kappa}\frac{1}{r^3}\xi^3 e^{-\xi^2} \qquad (6)$$

Where C is the fluid diffusivity, r is the distance between the source and the field point and the other notations are the same as those defined previously; $\xi = \frac{r}{2\sqrt{c(t-t')}}$.

For any distribution of the fluid source intensity $q_f(x',y',t')$ at the fracture surface, A, the resultant pressure in the reservoir at time t is given by

$$p(x,y,z,t) = \int_0^t\int_A q_f(x',y',t')p^{si}(x-x',y-y',z,t-t')\,dx'dy'dt' \qquad (7)$$

Likewise, given $q_f(x',y',t')$, the displacements and stresses in the reservoir can be calculated by (Cheng and Detournay, 1998):

$$\begin{Bmatrix}u_i(x,y,z,t)\\ \sigma_{ij}(x,y,z,t)\end{Bmatrix} = \int_0^t\int_A q_f(x',y',t')\begin{Bmatrix}u^{si}(x-x',y-y',z,t-t')\\ \sigma_{ij}^{si}(x-x',y-y',z,t-t')\end{Bmatrix}dx'dy'dt' \qquad (8)$$

Where u^{si} and σ_{ij}^{si} are the displacement and stress components induced by an instantaneous unit source.

To solve the present problem, we apply Eq. (7) on the fracture plane, i.e., let z=0 and $x, y \in A$:

$$p(X,0,t) = \int_0^t\int_A q_f(x',y',t')p^{si}(x-x',y-y',0,t-t')\,dx'dy'dt' \qquad (9)$$

Eqs. (5) and (9) can be solved together to obtain $p(x,y,0,t)$ and $q_f(x,y,t)$.

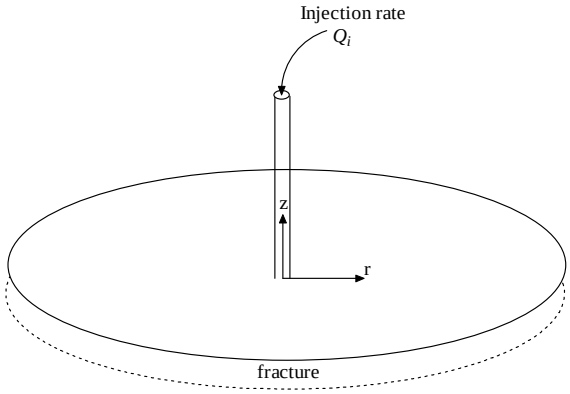

Figure. 1. . Fluid injection into an infinite radial fracture.

NUMERICAL FORMULATIONS

In this paper, we use Eqs. (5) and (9) together to obtain the fluid pressures in the fracture and the intensity of the distributed fluid sources on the fracture. The finite element method is used to solve the fluid flow in the fracture, and the boundary integral equation method is used for the three-dimensional pore fluid diffusion and stresses in the reservoir.

In the numerical model, the fracture plane is discretized into *M* elements. We let:

$$p^{(m)} = \mathbf{N}^{(m)}\tilde{\mathbf{p}} \quad \text{and } q_f{}^{(m)} = \mathbf{N}^{(m)}\tilde{\mathbf{q}}_f \qquad (10)$$

The following finite element formulae is derived from Eq. (5) by using the Galerkin method:

$$\mathbf{A}_1\tilde{\mathbf{p}}(t) + \mathbf{A}_2\tilde{\mathbf{q}}_f(t) = \mathbf{B}_1(t) \qquad (11)$$

$$\mathbf{A}_1 = \sum_{m=1}^{M}\int_{A_e} \nabla^T\mathbf{N}^{(m)} w(x,y) \nabla\mathbf{N}^{(m)} dA \qquad (12)$$

$$\mathbf{A}_2 = 12\mu\sum_{m=1}^{M}\int_{A_e} \mathbf{N}^{(m)T}\mathbf{N}^{(m)} dA \qquad (13)$$

$$\mathbf{B}_1 = 12\mu\mathbf{N}^{(i)T}\Big|_{(x_i,y_i)} Q_i(t) + 12\mu\mathbf{N}^{(e)T}\Big|_{(x_e,y_e)} Q_e(t) \qquad (14)$$

in which M is the total number of the elements on the fracture plane, $\mathbf{N}^{(i)T}\Big|_{(x_i,y_i)}$ denote the shape functions at the fluid injection point which is located at (x_i, y_i) within element i, $\mathbf{N}^{(e)T}\Big|_{(x_e,y_e)}$ denote the shape functions at the fluid extraction point which is located at (x_e, y_e) within element e. In Eq.(11), all $\tilde{\mathbf{p}}(t)$, $\tilde{\mathbf{q}}_f(t)$ and $\mathbf{B}_1(t)$ are functions of time, which means Eq. (11) should be obeyed all the time for the present problem.

Eq. (9) is discretized using the boundary element method, in which the convolution algorithm (Dargush and Banerjee, 1989) is used in the temporal domain and the same element mesh in the finite element formulation is used in the spatial domain. Eventually, we obtain:

$$p(x,y,0,t) = \left[\sum_{m=1}^{M}\int_{A_e} \mathbf{N}^{(m)} p_1^{sc}(x-x', y-y', 0)\, dx'dy'\right]\tilde{\mathbf{q}}_f(N\Delta t) + \sum_{n=1}^{N-1}\left[\sum_{m=1}^{M}\int_{A_e} \mathbf{N}^{(m)} p_{N-n+1}^{sc}(x-x', y-y', 0)\, dx'dy'\right]\tilde{\mathbf{q}}_f(n\Delta t) \qquad (15)$$

where the time from 0 to t is divided into N equal increments of Δt, p^{sc} is the continuous pore pressure solution induced by the unit fluid source intensity, and p_1^{sc} and p_n^{sc} are defined as follows:

$$p_1^{sc}(...) = p^{sc}(x-x', y-y', 0, \Delta t) \qquad (16)$$

$$p_n^{sc}(...) = p^{sc}(x-x', y-y', 0, n\Delta t) - p^{sc}(x-x', y-y', 0, (n-1)\Delta t) \qquad (17)$$

Applying Eq. (15) on all element nodes at the fracture plane, we obtain:

$$\tilde{\mathbf{p}}(t) = \mathbf{A}_3\tilde{\mathbf{q}}_f(t) + \mathbf{B}_2 \qquad (18)$$

Where:

$$\mathbf{A}_3 = \begin{bmatrix} \sum_{m=1}^{M}\int_{A_e} \mathbf{N}^{(m)} p_1^{sc}(x_1-x', y_1-y', 0)\, dx'dy' \\ \sum_{m=1}^{M}\int_{A_e} \mathbf{N}^{(m)} p_1^{sc}(x_2-x', y_2-y', 0)\, dx'dy' \\ \vdots \\ \sum_{m=1}^{M}\int_{A_e} \mathbf{N}^{(m)} p_1^{sc}(x_l-x', y_l-y', 0)\, dx'dy' \end{bmatrix} \qquad (19)$$

$$\mathbf{B}_2 = \sum_{n=1}^{N-1}\begin{bmatrix} \sum_{m=1}^{M}\int_{A_e} \mathbf{N}^{(m)} p_{N-n+1}^{sc}(x_1-x', y_1-y', 0)\, dx'dy' \\ \sum_{m=1}^{M}\int_{A_e} \mathbf{N}^{(m)} p_{N-n+1}^{sc}(x_2-x', y_2-y', 0)\, dx'dy' \\ \vdots \\ \sum_{m=1}^{M}\int_{A_e} \mathbf{N}^{(m)} p_{N-n+1}^{sc}(x_l-x', y_l-y', 0)\, dx'dy' \end{bmatrix}\tilde{\mathbf{q}}(n\Delta t) \qquad (20)$$

in which l is the total number of element nodes, and $t = N\Delta t$. By substituting Eq. (18) into Eq.(11), we obtain

$$\left(\mathbf{A}_1\mathbf{A}_3+\mathbf{A}_2\right)\tilde{\mathbf{q}}_f\left(t\right)=\mathbf{B}_1-\mathbf{A}_1\mathbf{B}_2 \qquad (21)$$

where all $\mathbf{A}_1$, $\mathbf{A}_2$, $\mathbf{A}_3$, $\mathbf{B}_1$ and $\mathbf{B}_2$ can be calculated directly. Therefore, Eq. (21) can be used to obtain the fluid source intensity $\tilde{\mathbf{q}}_f\left(t\right)$ at the fracture. Thereafter, $\tilde{\mathbf{p}}\left(t\right)$ can be solved through Eq. (18). Further, once $\tilde{\mathbf{q}}_f\left(t\right)$ is obtained, the pore pressures, displacements and stresses at any place and time in the reservoir induced by the fluid leak-off could be calculated by using Eq. (8) for which the boundary element method should also be adopted.

EXAMPLES AND ANALYSIS

The poroelastic effect of injection into a fracture is considered. No analytical solution is available for the three-dimensional version of the problem. However, using the assumption of one-dimensional fluid loss perpendicular to the fracture surface, Nygren and Ghassemi (2006) presented an analytical solution of the pore pressures in the fracture and reservoir for the problem of water injection into an infinite radial fracture (see Fig. 2). Thus, the results from the present numerical model are compared to those from the analytical solutions in Nygren and Ghassemi (2006). The parameters used in the comparison are listed in Table 1.

Table 1. Parameters used in the comparisons between the numerical model and analytical model.

Parameter	Value
Fluid injection rate Q (l/s)	20
Fracture aperture w_0 (mm)	1
Wellbore radius r_{well} (m)	0.1
Shear modulus G (MPa)	7000
Poisson's ratio ν	0.2
Fluid viscosity μ_f (N.s/m^2)	0.001
Fluid diffusivity c_f (m^2/s)	1.0×10^{-3}
Biot's coefficient α	0.75
Fluid density ρ_f (kg/m^3)	1000
Rock density ρ_r (kg/m^3)	2300
Rock permeability κ (m^2)	1.0×10^{-16}

Figure 2 shows a comparison between the analytical and numerical results for an injection time of 6 hours. The fluid pore pressures at the height of 0m, 5m, and 10m above the fracture along the radial direction of the fracture are presented.

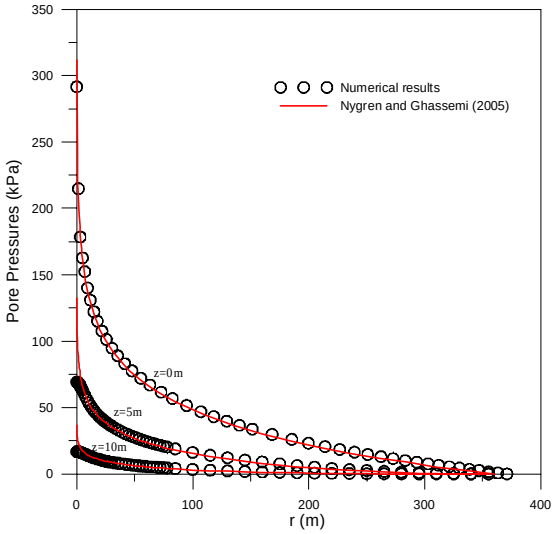

Figure. 2. Comparisons of pore pressures in reservoir from present numerical model and analytical model by Nygren and Ghassemi (2006) when fluid injection time is 6 hours.

It is observed that the numerical results for the pore pressures in the reservoir near the fluid injection well are much smaller than those from the analytical method. The discrepancy is caused by the fact that the one-dimensional fluid diffusion is assumed in the analytical method, however, the fluid pressure in the fracture near the well varies very fast in the radial direction. Far away from the well, the numerical results agree very well with the analytical results.

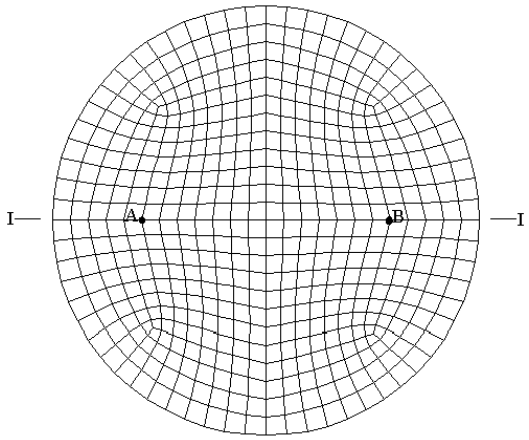

Figure. 3. Discretization of the circular fracture, where A is the fluid injection well and B is the fluid extraction well.

Next, we study a circular fracture with a radius of 50m by using the numerical model. As shown in

Figure 3, fluid is injected into well A(-30, 0) at a prescribed rate, and extracted out from well B(30, 0) at a given pressure. The circumference of the fracture is assumed to be impermeable. The fluid injection rate is assumed to be 20 l/m^3 and the fluid pressure in well B is assumed to be 0.5MPa. The initial in-situ stresses and pore pressure in the formation are assumed to be zero. The other parameters used here are the same as those in Table 1.

Fig. 4 shows the fluid pressures in the fracture for an injection time of 3 days. It is observed that the fluid pressures near the injection well are much larger than those near the extraction well. The fluid pressure profile in the fracture remains nearly the same with the elapse of time. Fig. 5 shows the pore fluid pressure in the rock matrix for zx-plane (I-I cross section, see Fig. 3). In the figure, the pore pressures dissipate from the fracture surface to the far-field with the elapse of the time. In the present work, we also calculate the fluid pressure in the fracture without considering the fluid leak-off. It is found that the influence of the fluid leak-off on the fluid pressure in the fracture is negligible if the reservoir permeability is relatively low (as fluid flow rate from the fracture into the reservoir is very low and aperture variation is not significant).

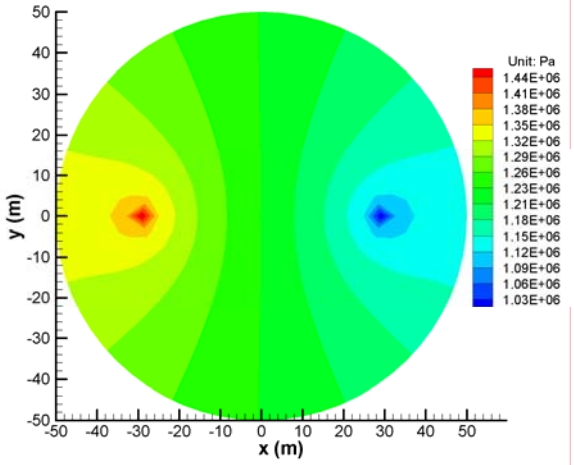

Figure. 4. pressures at fracture for fluid injection times of 3 days.

Fig. 6 shows the vertical total stress σ_{zz}, the component that is perpendicular to the fracture at its surface. They are compressive as expected (shown as negative). The highest value and the lowest value are respectively at the locations of the injection well and the extraction well. σ_{zz} increases with the increasing fluid injection time. When the fluid injection time is long, the distribution of σ_{zz} is similar to that of the fluid pressures in the fracture except that the absolute value of σ_{zz} is smaller. Fig. 7 shows the total stress σ_{zz}, at the cross section I-I. It is observed that the

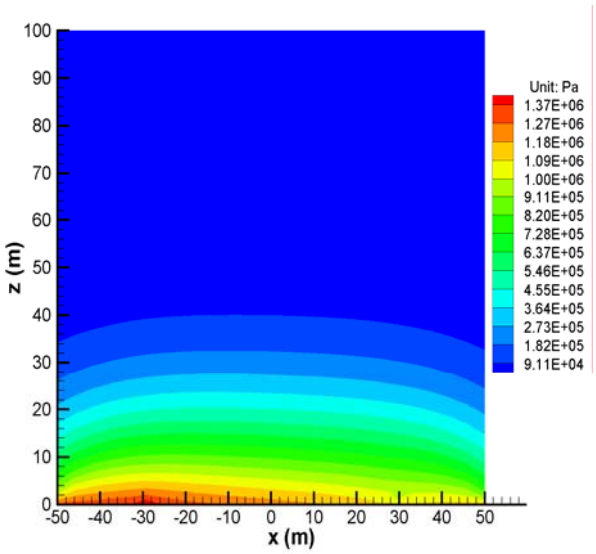

Figure. 5. Pore fluid pressures at I-I cross section for 3 days of injection.

compressive total stresses in the reservoir increase with time. As the deformation of the reservoir is controlled by the effective stress, we present the distributions of vertical effective stress, σ'_{zz}, which is calculated using the relation $\sigma'_{zz}=(\sigma_{zz}-\alpha)$, where α is the Biot's effective stress coefficient, and p is the pore fluid pressure.

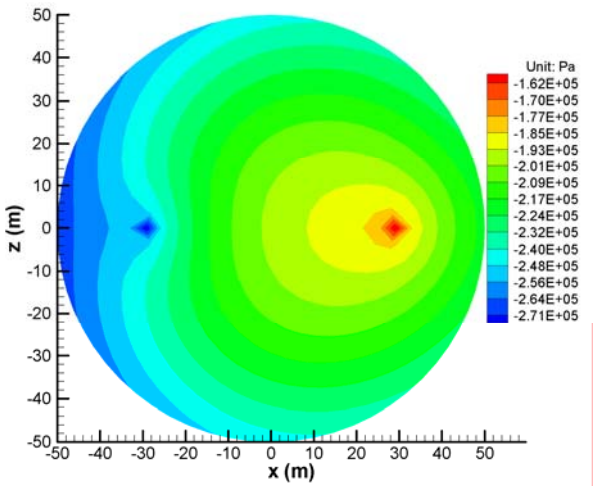

Figure. 6. Total vertical stress at fracture surface after 3 days.

The effective vertical stress, σ'_{zz} on the fracture surface corresponding to 3 days are shown in Fig. 8. From the figure, it is observed that as expected the effective stresses induced by the fluid leak-off are tensile, which results in fracture closure. This phenomenon has been noted by Ghassemi and Zhang (2006) for the problem of uniform pressure in line fractures.

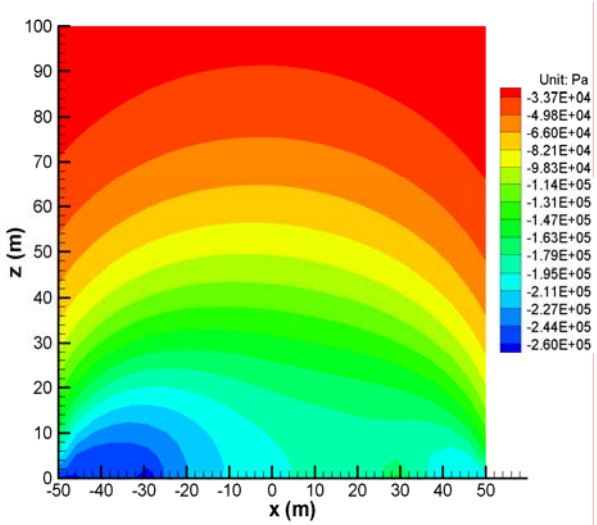

Figure. 7. Total vertical stress at I-I cross section after 3 days.

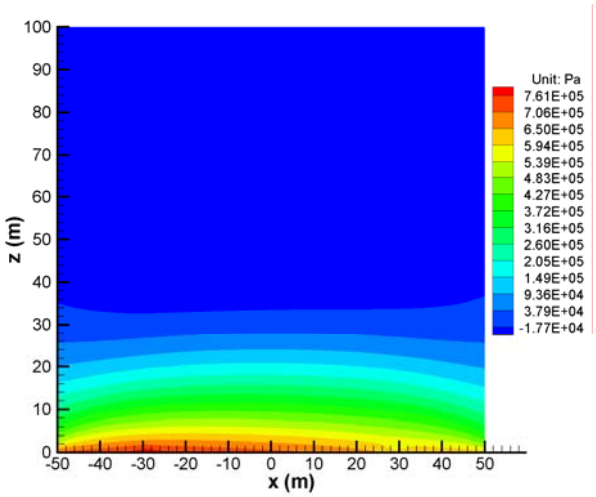

Figure. 8. Effective vertical stress at I-I cross section after 3 days.

The largest and smallest σ'_{zz} are at the locations of the injection well and extraction well, respectively. Fig. 9 shows the distributions of σ'_{zz} at the cross section I-I after 180 days. It is observed that the value of σ'_{zz} extends to a relatively far place with the elapse of the time.

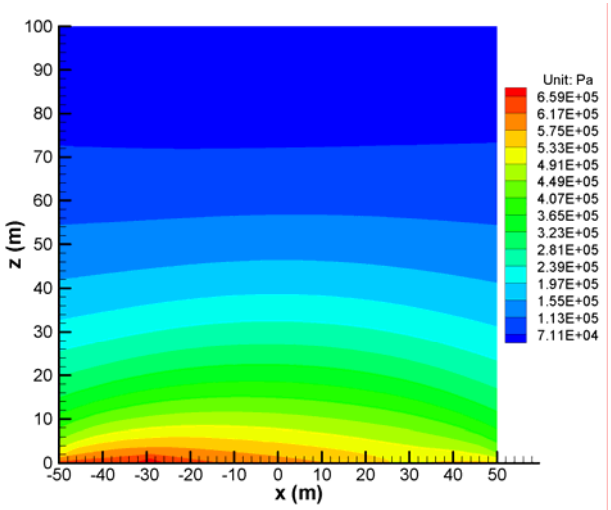

Figure. 9. Effective vertical stress at I-I cross section after 180 days.

CONCLUSIONS

A three-dimensional numerical model has been developed to investigate the poroelastic effect of the fluid injection into a geothermal reservoir. The three-dimensional pore fluid diffusion in the reservoir and the induced stresses are modeled by the boundary integral equation method. The numerical results have been compared with the analytical solutions for an infinite radial fracture problem. Good agreement was observed between the numerical and analytical results. Thereafter, the model was used to study a circular fracture problem with two wells for the better understanding the effect of the fluid leak-off into the reservoir. The impact of fluid leak-off on the fluid pressures in the fracture is small for a low permeability rock. However the fluid leak-off from the fracture into the reservoir induces pore pressure and stress in the reservoir. The total stresses in the reservoir induced by the fluid leak-off are compressive. However, the effective stresses induced by the leak-off are tensile.

REFERENCES

Cornet, F.H. and Jianmin, Y. (1995). "Analysis of induced seismicity for stress field determination and pore pressure mapping," *Pure and Applied Geophys*., **145**(3/4), 677-700.

Crouch, S.L. and Starfield, A.M. (1983). Boundary element methods in solid mechanics, Allen Unwin, NY.

Dargush, G. F. and Banerjee, P. K. (1989). "A time domain boundary element method for poroelasticity," Int. *J. Numer. Methods Eng*., 28, 2423-2449.

Detournay, E. and Cheng, A. H.-D. (1993). Fundamentals of poroelasticity. In: Comprehensive rock engineering: principles, practice and projects, analysis and design method. Vol 2. Editor: C. Fairhurst. Pergamon Press, Oxford. 113-171.

Ghassemi, A. and Roegiers, J.-C. (1996). "A three-dimensional poroelastic hydraulic fracture simulator using the displacement discontinuity method," Proc.

2nd North American Rock Mech. Symposium, Montreal, Ca, **1**, 982-987.

Ghassemi, A., Tarasovs, S. and Cheng, A. H.-D. (2007). "A Three-Dimensional Study of the Effects of thermo-mechanical loads on fracture slip in enhanced geothermal reservoir," *Int. J. Rock Mechanics & Min Sci*., Vol. 44 , pp. 1132–1148.

Ghassemi, A. and Zhang, Q. (2006). "Poro-thermoelastic response of a stationary crack using the displacement discontinuity method," *ASCE J. Engineering Mechanics*, **132**(1), 26-33.

Gutierrez-Negrin L.C.A. and Quijano-Leon J.L. (2003). "Analysis of seismicity in the Los Humeros, Mexico, geothermal field," Geothermal Resources Council Transactions, **28**.

Kohl, T., Evans, K.F., Hopkirk, R.J. and Ryback, L. (1995). "Coupled hydraulic, thermal, and mechanical considerations for the simulation of hot dry rock reservoirs," *Geothermics*, 24, 345-359.

Nygren, A. and Ghassemi, A. (2006). "Coupled Poroelastic and Thermoelastic Effects of Injection into a Geothermal Reservoir," 40th U.S. Rock Mech. Symp., Golden, CO.

Nygren, A., Ghassemi, A. and Cheng A.H.-D. (2005). "Effects of cold-water injection on fracture aperture and injection pressure," GRC Annual Conf., Reno, Nevada.

Peasron, C. (1981). "The relationship between micro-seismicity and high pore pressure during hydraulic stimulation experiments in low permeability rocks," *J. Geophy. Res.*, 86, B9, 7855.

Perkins, T.K. and Gonzalez, J.A. (1985). "The effect of thermoelastic stresses on injection well fracturing," SPE 11332.

Pine R. J. and Batchelor, A.S. (1984). "Downward migration of shearing in jointed rock during hydraulic injections," *Int. J. Rock Mech. Min. Sci. & Geomech*. Abstr. **21**(5), 249-63.

Warpinski, N.R. Wolhart, S.L. and Wright, C.A. (2001). "Analysis and prediction of microseismicity induced by hydraulic fracturing," SPE 71649.